International Journal of Energy Horizon 02 (2025) 61-69

International Journal of Energy Horizon

journal homepage: https://dergipark.org.tr/tr/pub/ijeh

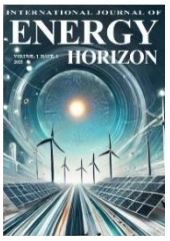

Research Article

Improvement of Haber–Bosch process for low carbon ammonia production through hybrid hydrogen recovery and energy recycling

Akın Doğan[1], Erhan Kayabasi[1,2,*]

[1] Karabuk University, Engineering Faculty, Mechanical Engineering Department 78050, Karabuk, Turkey
[2] Karabuk University, Iron and Steel Institute, Karabuk, Turkey
[1]ORCID No: 0009-0009-4564-9536
[2]ORCID No: 0000-0002-3603-6211

ARTICLE INFO

Article History:

Received:22 September 2025
Revised:7 October 2025
Accepted:2 November 2025
Available online:30 November 2025

Keywords:

Green ammonia
Haber–Bosch
Energy recovery
Hybrid hydrogen production

ABSTRACT

The energy-intensive nature of the Haber–Bosch process necessitates the development of self-sustaining synthesis systems. This study proposes a novel configuration integrating a hybrid hydrogen production method and a closed-loop energy recovery system to minimize external energy dependence and carbon emissions. Hydrogen is generated through the water–gas shift reaction using water molecules instead of natural gas, while the by-products carbon monoxide and carbon dioxide are reintegrated into the system to recover energy via turbine units. A detailed process simulation was conducted to evaluate the effects of temperature and pressure on ammonia yield and conversion rates. The results indicate that the optimal operating conditions (≈300°C, 30 bar) maximize both conversion efficiency and energy recovery, enabling the process to fully meet its energy demand internally. Compared to conventional systems, the proposed design reduces overall energy consumption and carbon footprint by transforming waste gases into usable electricity. The findings present a sustainable framework for green ammonia synthesis, emphasizing the significance of integrated hydrogen recovery and energy recycling.

1. INTRODUCTION

Global energy demand is projected to increase by approximately 80% by 2050, driven by rapid population growth and industrial expansion. This surge in energy consumption is directly linked to rising environmental pollution and the accelerated depletion of fossil fuel reserves. Consequently, the utilization of renewable energy sources has emerged as a critical factor in mitigating fossil fuel consumption and reducing environmental degradation [1]. As fossil fuel reserves continue to decline, the search for alternative and synthetic fuels has gained prominence, with ammonia emerging as a promising candidate. There are several key reasons why synthetically produced ammonia is considered a viable alternative fuel. Firstly, ammonia possesses a high energy density, making it an efficient energy storage and transportation medium [2]. Additionally, ammonia is one of the most widely used chemicals in the chemical industry, with its primary applications including agricultural fertilizers, refrigerants in cooling systems, cleaning products, and an alternative fuel for internal combustion engines [3].

Ammonia production has been predominantly based on the Haber-Bosch process, developed by Fritz Haber and Carl Bosch in the early 1900s, which marked the beginning of large-scale industrial ammonia synthesis. In terms of production volume, ammonia ranks as the second most-produced chemical worldwide, with an annual output of approximately 200 million tons. Notably, approximately 85% of ammonia production is allocated to the manufacturing of fertilizers such as urea, ammonium sulfate, and ammonium nitrate [4,5]. The Haber-Bosch process involves the reaction of gaseous nitrogen (N_2) and hydrogen (H_2) under high pressure (100–450 bar) and elevated temperatures (300–500°C) to synthesize ammonia [6]. Given these fundamental advantages, ammonia has recently garnered substantial international attention. The Haber-Bosch process involves the production of hydrogen through the utilization of hydrocarbons such as coal, natural gas, or naphtha, which is subsequently combined with nitrogen gas extracted from atmospheric air. Due to its high reactivity, ammonia serves as a fundamental building block in the synthesis of numerous nitrogen-containing

*Corresponding author
E-mail address: erhankayabasi@karabuk.edu.tr
journal homepage: https://dergipark.org.tr/tr/pub/ijeh

compounds [7]. However, current ammonia production processes result in the release of approximately 2.7 to 3.4 tons of carbon dioxide per ton of ammonia produced, primarily due to the use of natural gas or coal as carbon sources. Additionally, ammonia synthesis accounts for approximately 1–2% of global energy consumption [8]. In response to growing environmental concerns and the escalating effects of climate change, there has been an increasing interest in low-carbon ammonia production methods. One such approach, known as "green ammonia production," involves the electrolysis of water (H_2O) to obtain hydrogen, which is subsequently reacted with nitrogen using renewable energy sources [4]. Although green ammonia production is not a novel concept, it was historically employed in Norway from the late 1920s to the 1990s through the utilization of hydroelectric power for sustainable hydrogen production via the Atmospheric Electrolysis Cell (AEC) process [9]. Compared to conventional methods, this approach significantly reduces greenhouse gas emissions. In a study by Duncan A. Nowicki, a conceptual design was proposed for a small-scale green ammonia plant utilizing the Haber-Bosch cycle, in which hydrogen was produced via a solid oxide electrolyzer and nitrogen was purified from atmospheric air. The operational efficiency of the system was reported as 52.12%, yielding results comparable to those of the cryogenic air separation unit (ASU) reference system, which achieved an efficiency of 52.89%. The specific energy consumption for ammonia synthesis was documented as 9.94 kWh/kgNH_3. Despite these promising results, further improvements in system design remain necessary. For instance, optimizing heat integration by utilizing waste heat from oxygen pumps to supply the steam required for the electrolyzer could enhance overall system efficiency while simultaneously reducing energy consumption [10]. Another alternative, "blue ammonia," integrates fossil fuel-based ammonia production with carbon capture and storage (CCS) technologies. While this approach has the potential to significantly reduce carbon emissions, the process still involves components that contribute to considerable levels of emissions. Furthermore, both green and blue ammonia production methods present substantial technical and economic challenges, necessitating comprehensive evaluation and the development of alternative systems [7]. Blue ammonia has the potential to serve as a crucial tool in addressing the need to reduce carbon emissions. Most research on blue ammonia has primarily focused on advancing new reforming techniques aimed at minimizing CO_2 emissions [11]. One such example is the process designed by Martínez et al., which utilizes the oxidation properties of CaCu to enhance the efficiency of ammonia production while simultaneously reducing CO2 emissions through the formation of CaCO3 [12]. Gray ammonia production plays a significant role in wastewater management and the mitigation of environmental impacts. In this context, ammonia recovery and utilization can offer both economic and ecological benefits. However, due to its potential effects on air quality, ammonia must be carefully managed to align with environmental sustainability goals [13]. Research on gray ammonia primarily focuses on its environmental implications, as well as its industrial applications and possible recovery methods. Advancements in this field present significant opportunities for improving both energy efficiency and waste management [14]. Turquoise ammonia has emerged as a critical component in sustainable energy production and environmental management. Traditional ammonia production techniques, which rely on hydrogen derived from natural gas, result in significant carbon dioxide emissions. In contrast, turquoise ammonia is synthesized through the reaction of hydrogen with methane, a process designed to significantly reduce carbon emissions. This approach integrates carbon capture and storage (CCS), thereby minimizing its environmental footprint. Turquoise ammonia has various applications, including its use as a fertilizer in agriculture, as well as in transportation and energy storage. Additionally, wastewater treatment and bioenergy production represent essential aspects of this production method [15,16]. Given the limitations of green and blue ammonia production processes particularly regarding carbon emissions, electricity sources, and hydrogen supply, it is evident that several aspects require further development. This study investigates the potential for replacing these shortcomings with alternative resources and restructuring the production system accordingly. In this study, the mass and energy balance of an ammonia production process is analyzed, with the primary objectives of reducing the energy demand of the process, recovering mass flows within the system, and ultimately minimizing both energy losses and CO_2 emissions. By optimizing these parameters, the study aims to achieve the lowest possible energy and material consumption per unit of ammonia produced.

2. MATERIALS AND METHODS

The process simulation was developed in DWSIM. The water-gas shift reaction was modeled using an equilibrium reactor approach, based on the kinetics reported by [17], specifically utilizing the Langmuir-Hinshelwood type rate expression (Eq. 13). The ammonia synthesis reactor was modeled as a Plug-Flow Reactor (PFR) using the Temkin-Pyzhev kinetic model as implemented in DWSIM's built-in ammonia reactor module. The thermodynamic property package selected for the system was the Soave-Redlich-Kwong (SRK) equation of state, which is well-suited for high-pressure petrochemical and synthesis gas processes. The simulation convergence was achieved using the Boston-Britt inside-out method with a relative convergence tolerance of 1×10^{-6}.

The water-gas shift reaction is one of the most important methods used in the chemical industry for the production of pure hydrogen, particularly due to its efficiency and cost-effectiveness in large-scale applications such as ammonia synthesis. This process involves the reaction of carbon monoxide with steam, resulting in the formation of carbon dioxide and hydrogen.

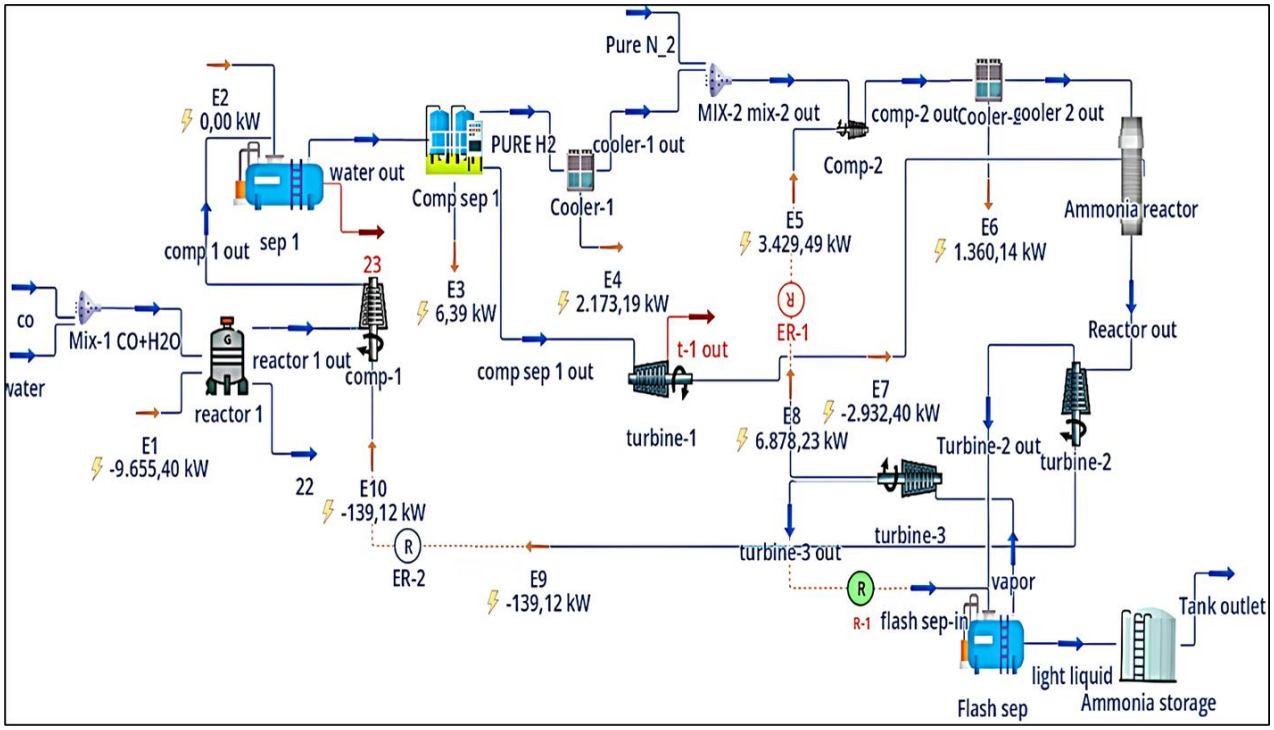

Figure 1. General layout of the proposed system.

The equilibrium reaction, with an equilibrium constant of 6.80 and a conversion rate of approximately 80%, plays a crucial role in hydrogen production. Initially, the steam and carbon monoxide flow rates are 100 mol/h and 25 mol/h, respectively. These reactants are mixed and sent to an equilibrium reactor, where they react in the vapor phase. Following the reaction, the vapor-phase products are directed to a compressor to reach the ideal operating pressure of 25 bar. The electrical energy required for the compressor is supplied by the system component named Turbine 3. The outlet stream is then directed to a separator, where 0.45 mol fraction of hydrogen is present in the vapor phase, while the liquid phase is discharged. The hydrogen stream is subsequently sent to a compound separation unit to obtain pure hydrogen, yielding approximately 1677 kmol/h of high-purity hydrogen. When the system component "Compound Separator 1" is utilized for hydrogen purification, it generates approximately 10.38 kWh of energy. The material stream discharged from the compound separation unit contains approximately 83% CO_2 and 16% CO at a pressure of 25 bar. Given its high pressure, this stream is utilized to generate the electrical energy required for the ammonia reactor. The outlet stream from the compound separator, referred to as "compound separator discharge," is directed to Turbine 2 to reduce its pressure from 25 bar to 0.05 bar. This pressure reduction process yields approximately 4.987 MW of energy. The water-gas shift reaction, which is employed for pure hydrogen production, demonstrates a high level of efficiency and effectiveness, with an approximately 80% conversion rate [17]. Composition of NG in this study is as follows: CH_4 90.3%, C_2H_6 6.6%, C_3H_8 2.2%, C_4H_{10} 0.9%. Steam reforming reactions of CH_4 and the other C_nH_m hydrocarbons are represented by Eq.'s (1) and (2), respectively[18].

$$CH_4 + H_2O \leftrightarrow CO + 3H_2, \qquad \Delta H^0 = 206 \times 10^3 \frac{kJ}{kMol} \tag{1}$$

$$C_nH_m + nH_2O \leftrightarrow nCO + \left(n + \frac{m}{2}\right)H_2 \tag{2}$$

The development of a compact fuel reformer through process simulation and optimization necessitates accurate modeling of WGS reaction kinetics, which serve as a critical component. Numerous kinetic rate expressions have been proposed and examined to assess the water–gas shift reaction rate across different catalysts, as illustrated in Eq. (3)[18].

$$CO + H_2O \leftrightarrow CO_2 + H_2, \qquad \Delta H^0 = -41 \times 10^3\ kJ/kMol \tag{3}$$

The equilibrium relationship of reaction (1) and the corresponding temperature dependence of the equilibrium constant, K_{MSR} are expressed in Eqs. (4) and (5), respectively[18].

$$K_{msR} = \frac{y_{CO}y_{H_2}^3}{y_{cH_4}y_{H_{2O}}}P_t^2 \tag{4}$$

$$= 10^{\frac{-11650}{T(k)}+13.076} \tag{5}$$

Here, y denotes the mole fraction of a gaseous component, while P_t (bar) represents the total pressure of the reforming reaction. The equilibrium relationship for the WGS reaction (3) and the temperature dependence of the corresponding equilibrium constant, K_{WGS}, are defined as follows[18]:

$$K_{WGS} = \frac{y_{Co_2}y_{H_2}}{y_{CO}y_{H_2O}} \tag{6}$$

$$= 10^{\frac{1910}{T(K)}-1.784} \tag{7}$$

For a given temperature and pressure, the equilibrium conversion of CH_4 in the reaction (1) and the equilibrium reaction extent of the reaction (3) can be obtained by simultaneously solving the Eqs. (4) and (7) after replacing all the mole fraction terms with CH_4 conversion and WGS reaction extent according to each reaction stoichiometry. On the other hand, steam reforming conversions of the other C_2 hydrocarbons in the NGR are assumed as 100%. þ Heat of reaction in the reactions (1)e(3) including heats of combustion of NGB at temperature T(K) can be obtained as follows [18]:

$$\Delta H_r(T) = \Delta H_r^0 + \int_{298}^{T} \Delta C_p\, dT \tag{8}$$

where, ΔC_p can be calculated using the heat capacities of the species. As an instance, when 1 mole of C_nH_m is steam-reformed by reaction (2), ΔC_p is given by

$$\Delta C_p = \frac{n+m/2}{1}C_{p,H_2}\frac{n}{1}Cpc_0 - \frac{n}{1}c_{p,H_2O(g)} - C_{p,CnH_m} \tag{9}$$

Likewise, the difference of the standard enthalpy of formation, ΔH_r^0 can also be obtained using Eq. (9) by replacing Cp with ΔH^o. Stoichiometric amount of air needed for the combustion of NGB is calculated assuming complete combustion of NGB supplied to the burner. Actual feeding rate of combustion air is 1.1 times the stoichiometric amount. The flow rate and composition of CFG are also calculated using the stoichiometry. Combustion temperature (TBN) of NGB in the burner was assumed 300 C higher than the temperature (TSR) of steam reforming reaction in the catalyst bed. Most heat exchangers in Fig. 1 are installed to heat up NGR and WR using such hot gases as RFG and CFG. Particularly, HEX1 and HEX2 have a function to keep the temperatures of RFG entering HTS and LTS at 350 and 200 C, respectively. When hot and cold fluids flow counter-currently in a heat exchanger, the required heat transfer area, AHX, is calculated by [18]

$$A_{HX} = \frac{Q_{Hx}}{U\Delta T_{lm}} \tag{10}$$

where, Q_{HX} is a heat transfer rate (kJ/s), U is an overall heat transfer coefficient ($kJ/m^2/K/s$), and ΔT_{lm} is a logarithmic mean temperature difference (K):

$$\Delta T_{lm} = \frac{(T_{h,i}-T_{c,o})-(T_{h,o}-T_{c,i})}{\log\frac{T_{h,i}-T_{c,o}}{T_{h,o}-T_{c,i}}} \tag{11}$$

where, subscripts h and c indicate hot and cold fluids, respectively, and i and o indicate inlet and outlet positions of fluids in a heat exchanger. The process efficiency of hydrogen production was calculated using the low heating values (HLHV) of H_2 produced and NG consumed as follows[18]:

$$\eta = \frac{N_{H_2}H_{LHV,H_2}}{(N_{NGR}+N_{NGB})H_{LHV,NG}} \tag{12}$$

From the adsorptive mechanism, Langmuir–Hinshelwood type rate expressions can be derived. The following rate expression is derived from Yang–Hougen table when the surface reaction is assumed rate controlling [17]:

$$r_{CO} = k\frac{P_{H_2O}P_{CO}-P_{H_2}P_{CO_2}/K_P}{(1+K_1P_{CO}+K_2P_{H_2O}+K_3P_{CO_2}+K_4P_{H_2})^2} \tag{13}$$

For the redox mechanism an equation derived as following rate expression and confirmed its validity using Cu-Zn-Cr catalysts [17]:

$$r_{CO} = k\frac{P_{H_2O}P_{CO}-P_{H_2}P_{CO_2}/K_P}{AP_{H_2O}+P_{CO}} \tag{14}$$

Using a CuO/ZnO catalyst, another rate expression can be derived from the redox mechanism when a single path reaction model is assumed [17]:

$$r_{CO} = \frac{k_1k_2(P_{H_2O}P_{CO}-P_{H_2}P_{CO_2}/K_P)}{k_1P_{H_2O}+k_2P_{CO}+(k_{1\_}+k_{2\_})P_{CO_2}} \tag{15}$$

In contrast to those rate expressions from detailed reactions, mechanisms and rate determining steps, there are simple empirical rate expressions which do not consider any mechanism a simple reversible rate expression for CO conversion [17]:

$$r_{co} = k\left(P_{CO}P_{H_2O} - \frac{P_{CO_2}P_{H_2}}{K_P}\right) = kP_{CO}P_{H_2O}(1-\beta) \tag{16}$$

where

$$\beta = \frac{P_{CO_2}P_{H_2}}{P_{CO}P_{H_2O}K_{eq}} \tag{17}$$

Other research groups have reported that the water gas shift reaction is not a simple order reaction, especially at steam/CO ratios, and have tried to find proper exponent parameters in a power-law type equation [17]:

$$r_{CO} = kP_{co}^nP_{H_2O}^m(1-\beta) \tag{18}$$

From thermodynamic properties and relations, the equilibrium constant for the water gas shift reaction can be derived in a conventional way as shown in the following equation [17]:

$$\ln(K_{eq}) = \frac{5693.5}{T} + 1.077\ln T + 5.44\times10^{-4}T - 1.125\times10^{-7}T^2 - \frac{49170}{T^2} - 13.148 \tag{19}$$

where

$$K_{eq} \cong \frac{P_{CO_2}P_{H_2}}{P_{H_2O}P_{CO}} \tag{20}$$

a simpler equation for Keq is given as in Eq. (21):

$$K_{eq} = \exp\left(\frac{4577.8}{T} - 4.33\right) \tag{21}$$

Although the exothermic nature of the reaction suggests that lower temperatures would be advantageous, the specified temperature range provides an acceptable balance between ammonia yield and reaction kinetics. Even under these conditions, the conversion rate remains approximately 15–35% [10].

The pure hydrogen stream from the water-gas shift reactor is cooled to approximately 200°C in a heat exchanger (Cooler 1). The recovered thermal energy from this cooling process is integrated into the system's internal heat exchange network, reducing the overall heating demand. The hydrogen exiting Cooler 1 is then sent to Mixer 3, where it is combined with pure nitrogen sourced from the atmosphere. At the outlet of Mixer 3, the molar fractions of the gas stream are 0.77 for hydrogen and 0.23 for nitrogen. This gas stream is then fed into Compressor 2 to increase its pressure to the optimal level of 200 bar. The electrical power required for Compressor 2 is supplied by Turbine 3, which generates energy by reducing the pressure of high-pressure steam to the ideal operating pressure of 25 bar. The hydrogen-rich stream, after being pressurized in Compressor 2, is then sent to Cooler 1 to be adjusted to the appropriate reaction temperature (425°C). Due to the temperature difference, Cooler 1 also generates electrical energy. The cooled hydrogen is subsequently fed into the Ammonia Reactor, where the chemical reaction takes place to synthesize ammonia. The Ammonia Reactor's energy requirements are met through the electricity generated by expanding the high-pressure (25 bar) stream composed of 0.83 molar fraction CO_2 and 0.16 molar fraction CO from the Compound Separator to a lower pressure of 0.05 bar. The chemical reactions occurring within the ammonia reactor can be represented by the following formulas: The kinetic reactions are employed in Plug-Flow Reactors (PFRs) and Continuous-Stirred Tank Reactors (CSTRs). In these reactors, the relationship between molar concentration and reaction rate is expressed as follows:

$$\mathrm{FA} = \mathrm{FA}_0 + \int_0^V r_A dV \tag{23}$$

where FA is the molar flow of the A component and V is the reactor volume which forms a system of equations that must be solved using an ODE solver for each dV, since r_i depends on Ni. The reaction rate in the ammonia reactor is 0.004019 kmol/m³h, with conversion rates of 43.47% for hydrogen and 47.44% for nitrogen. At the reactor outlet, the material stream contains 55% hydrogen, 15% nitrogen, and 28% ammonia. To reach the optimal pressure level, this stream undergoes an expansion process in Turbine 2, where the pressure is reduced to 150 bar. This expansion generates electricity, which is subsequently utilized by the Energy Recycle Block to power Compressor 1, thereby reducing the overall energy costs of the system. The effluent from Turbine 2, still containing 55% hydrogen, 15% nitrogen, and 28% ammonia, is directed to the Flash Separator for separation of pure ammonia. At the Flash Separator outlet, a vapor-phase stream with a molar fraction of 0.95 is obtained. Given its high pressure, this vapor is sent to Turbine 3, where the pressure is lowered to 25 bar to facilitate energy recovery. The pressure drop in Turbine 3 generates electricity, which is reintegrated into the system to meet its power demands. To enhance ammonia production efficiency, the Turbine 3 outlet stream, containing residual hydrogen and ammonia, is recirculated back into the Flash Separator via the Recycle Block. This recycling process is essential for maximizing ammonia yield. Finally, the separated ammonia stream, free from hydrogen, nitrogen, methane, carbon dioxide, and carbon monoxide, is transferred to the Ammonia Storage Unit for further processing and utilization.

3. RESULT AND DISCUSSION

This graph illustrates the change in mass flow rate of pure nitrogen material stream with respect to pressure variation at different temperatures. For all temperature values, the mass flow rate increases as the pressure rises. However, beyond a pressure value of 30 bar, the slope of the curves decreases, indicating a reduced rate of increase. When examining different temperature values, it is observed that the mass flow rate increases as the temperature rises at a constant pressure. In other words, higher temperatures have an enhancing effect on mass flow rate. Between the pressure values of 30–35 bar, the mass flow rate reaches its maximum value, and the rate of increase diminishes after the 35 bar point. These findings suggest that temperature increase positively affects the mass flow rate, while pressure increase has a limiting effect beyond a certain threshold. The molar mass flow of ammonia according to the pressure increase was depicted in Fig. 2.

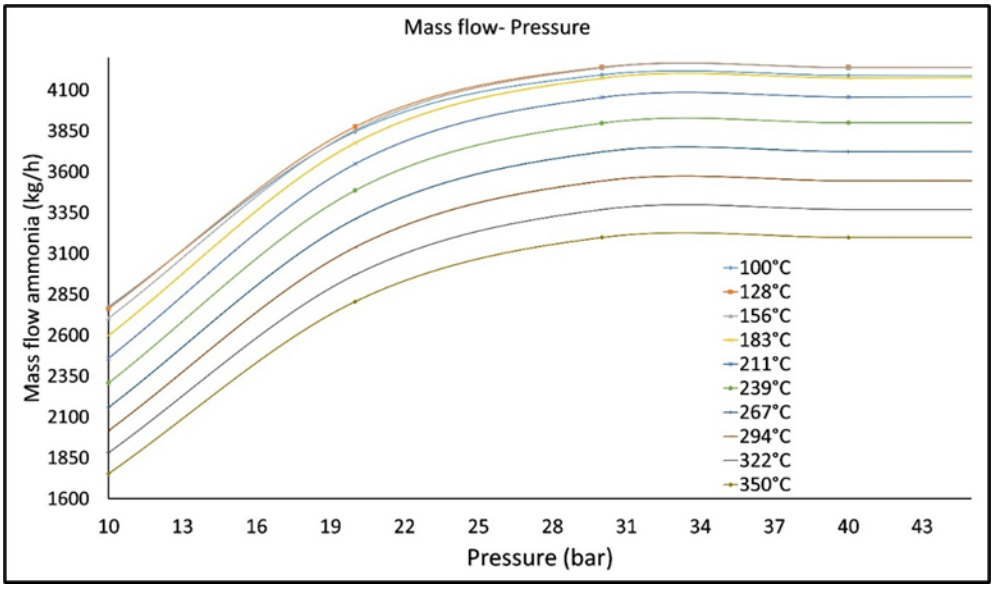

Figure 2. Molar mass flow of ammonia according to the pressure increase.

This graph presents a parametric study conducted to show the effect of increasing pressure values on the ammonia production efficiency of the system at different temperatures for pure nitrogen material flow. In all temperature values, the increase in pressure has a positive effect, boosting the efficiency; however, a pressure value of 30 bar represents the maximum point for most temperature curves. At pressure levels of 40-45 bar, the ammonia production efficiency stabilizes, showing a plateau across all temperature curves. Additionally, it is observed that as the temperature increases, the ammonia production efficiency also rises at the same pressure values. According to the parametric study, the system reaches its maximum efficiency at 322°C and 30 bar pressure. When examining all temperature values, it is evident that the 30 bar pressure ensures the maximum efficiency across all temperatures. In summary, efficiency improvement can be achieved with both temperature and pressure increases, but at higher pressures (above 30 bar), this effect becomes limited.

Figure 3 shows the mole fraction of ammonia (NH_3) formation as a function of pressure at different temperatures for pure nitrogen. It is generally observed that the ammonia mole fraction increases with the pressure value for each temperature. However, at a pressure value of 30 bar, it can be seen that the curves reach the maximum mole fraction value for most of the temperature conditions. Between 40-45 bar, all the curves flatten, indicating that the ammonia mole fraction stabilizes. Another result of the parametric study shows that, The observed decrease in ammonia mole fraction with increasing temperature, at a constant pressure, is a direct consequence of the exothermic nature of the ammonia synthesis reaction ($N_2 + 3H_2 \rightleftharpoons 2NH_3$, $\Delta H° = -92.4$ kJ/mol). According to Le Chatelier's principle, increasing the temperature shifts the equilibrium position towards the reactants, thereby lowering the equilibrium conversion and the resulting ammonia concentration. When examining the system at different temperature values, it is observed that the saturation value occurs at 30 bar. In conclusion, for optimum ammonia formation efficiency, lower temperatures should be preferred, and the pressure should not be increased beyond a certain level (approximately 30 bar).

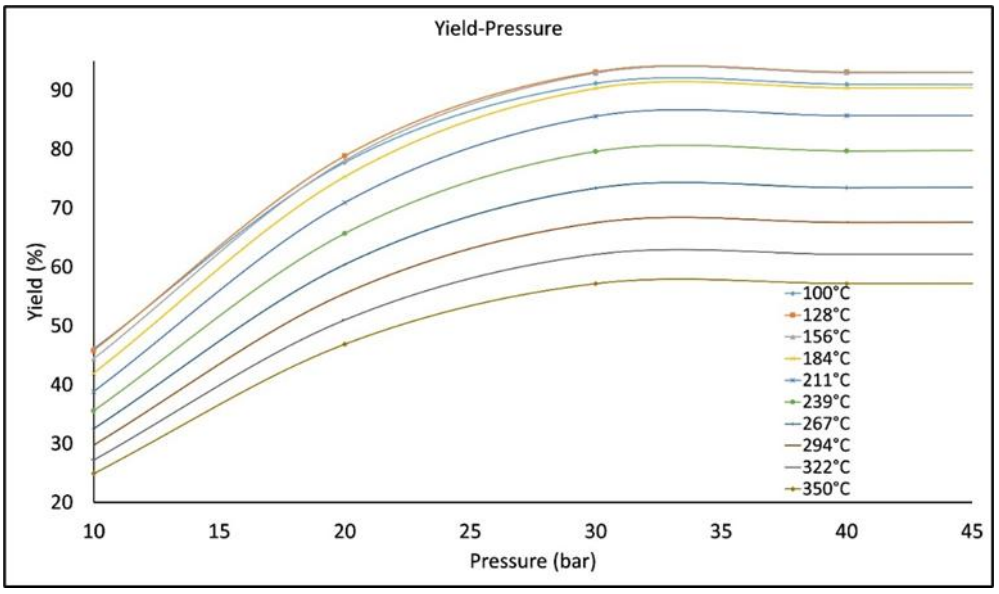

Figure 3. Yield versus reactor pressure under different reaction temperatures.

Figure 4 examines the relationship between temperature and ammonia mole fraction under different pressures (50, 90, and 100 bar). The data obtained shows a decreasing trend in the ammonia mole fraction as temperature increases. Especially at low temperature ranges (90°C-150°C), the mole fraction increases, and this trend continues up to approximately 150°C, after which it begins to decrease. As pressure increases, particularly at higher temperatures, it is observed that the rate of decrease in the ammonia mole fraction is relatively lower. This indicates the positive effect of pressure on the ammonia production reaction. Furthermore, for each pressure value in the graph, the maximum point of the ammonia mole fraction is observed to be between 130°C-150°C.

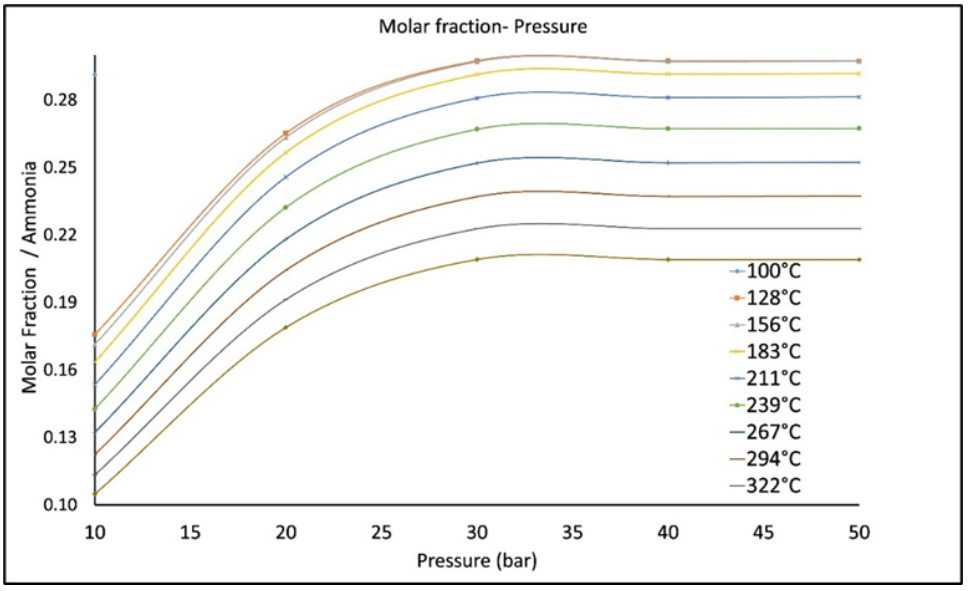

Figure 4. Molar fraction of ammonia under different reaction temperatures.

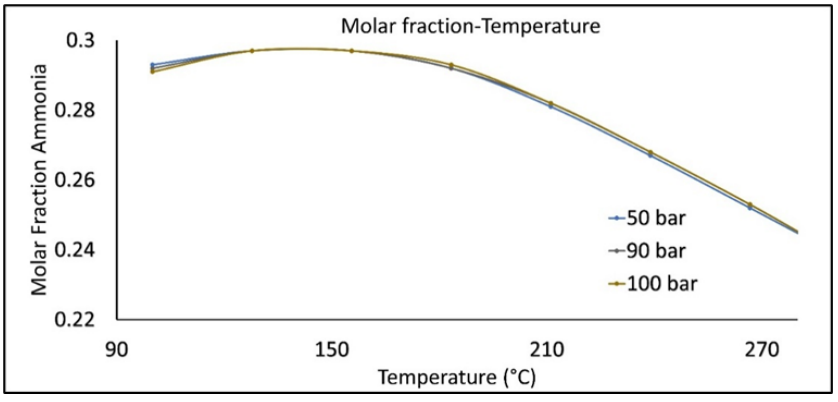

Figure 5. Molar fraction of ammonia for 50, 90 and 100 bar versus temperature increase.

In the Haber-Bosch process, the curves in Fig. 6 showing the effect of temperature changes on the hydrogen and nitrogen conversion rates during ammonia production indicates that temperature increases initially enhance the conversion rates of both gases. However, after a certain temperature, the conversion rates begin to decrease. As the temperature rises from 100°C to 300°C, the conversion rates for hydrogen and nitrogen reach 45% and 47.8%, respectively. The increase in conversion rates within this temperature range is due to the more favorable reaction kinetics under these conditions. However, when the temperature exceeds 200°C, a noticeable decrease in both hydrogen and nitrogen conversion rates is observed. This decline is attributed to the exothermic nature of the ammonia synthesis reaction, and according to Le Chatelier's Principle, the temperature increase shifts the system's equilibrium in the opposite direction, inhibiting ammonia formation. While higher temperatures accelerate the reaction kinetics, the thermodynamic equilibrium moves unfavorably towards ammonia decomposition, resulting in a decrease in conversion rates. The optimum temperature in the graph is identified around 300°C; however, in industrial applications, higher temperatures and pressures are preferred to increase reaction rates and efficiency. This situation highlights the complex interplay between kinetic and thermodynamic factors on ammonia production. Therefore, while ammonia formation is thermodynamically favored at lower temperatures, higher temperatures lead to the dominance of the reverse reaction, reducing the conversion rates of the gases.

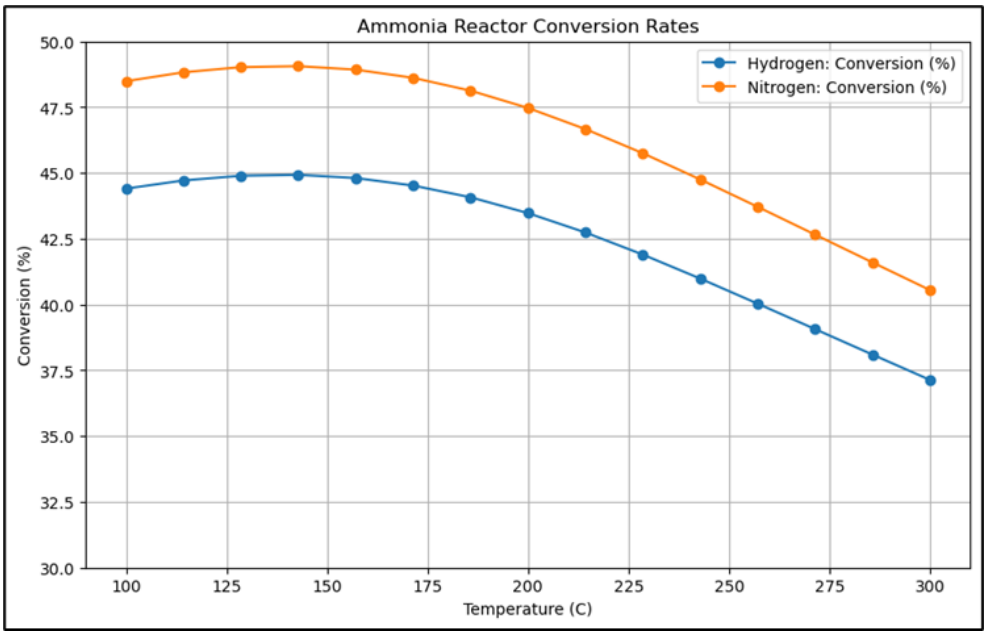

Figure 6. Ammonia conversion rates versus temperature

Fig. 7 examines the effect of pressure on hydrogen and nitrogen conversion rates during ammonia production in the Haber-Bosch process. Experimental data were obtained by measuring hydrogen and nitrogen conversion rates in the range of 0-50 bar. The conversion rate of hydrogen increases with pressure, starting at 10% and reaching 50% at 50 bar. The increase in hydrogen and nitrogen conversion rates with pressure is attributed to the decrease in the number of moles during the ammonia synthesis reaction. According to Le Chatelier's principle and the reaction equilibrium, higher pressures favor the forward reaction, leading to higher equilibrium conversions. Similarly, the conversion rate of nitrogen also increases with pressure, starting at 29% and reaching 45% at 50 bar. The conversion rate of nitrogen increases more rapidly at lower pressures, but the rate of increase slows down at higher pressures. The variation of hydrogen and nitrogen conversion rates with pressure emphasizes the importance of pressure control in the ammonia production process and highlights its role as a factor to consider in terms of energy efficiency. These findings suggest that pressure optimization in the ammonia production process could increase energy efficiency and reduce production costs. The data obtained can be used to improve energy efficiency and determine optimal operating conditions in industrial applications.

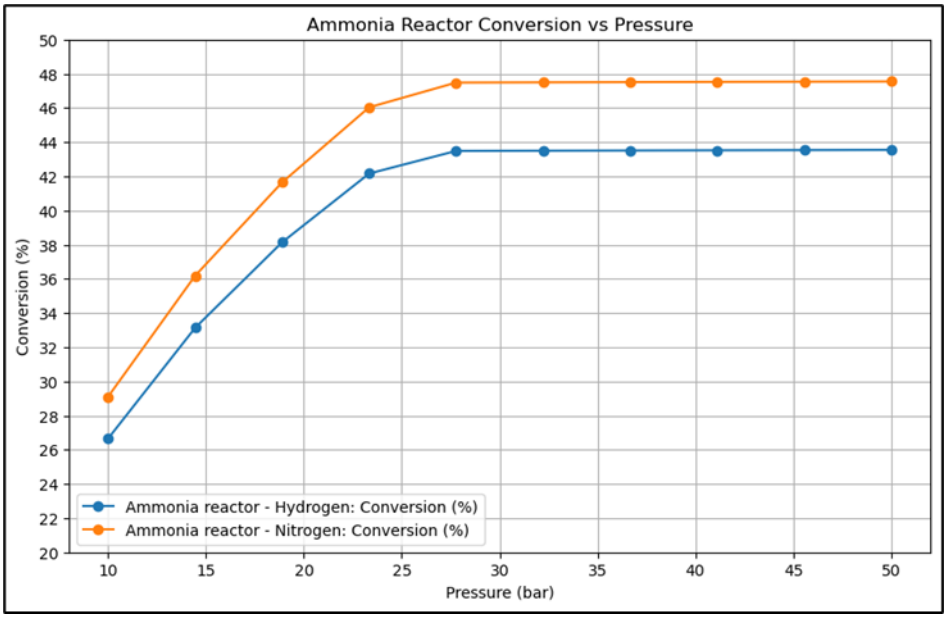

Figure 7. Ammonia reactor conversion versus pressure increase.

In Fig. 8, the relationship between temperature and ammonia yield (%) has been examined under various pressure values (40, 60, 80, and 100 bar). The data show that as temperature increases, the ammonia yield also increases, reaching a maximum at a specific temperature (145°C), after which the yield decreases as the temperature continues to rise. This behavior indicates that the highest yield values in the ammonia production process occur between 130°C and 150°C, marking the optimum temperature range. As pressure increases, relatively higher values of yield are observed, reflecting the positive effect of pressure on ammonia yield. However, even at high pressures, a decline in yield is observed when the temperature exceeds 150°C, indicating that excessive temperatures disrupt the reaction equilibrium. These results emphasize the importance of carefully selecting appropriate temperature and pressure conditions to achieve optimal ammonia yield and highlight the critical role of process parameters in production efficiency.

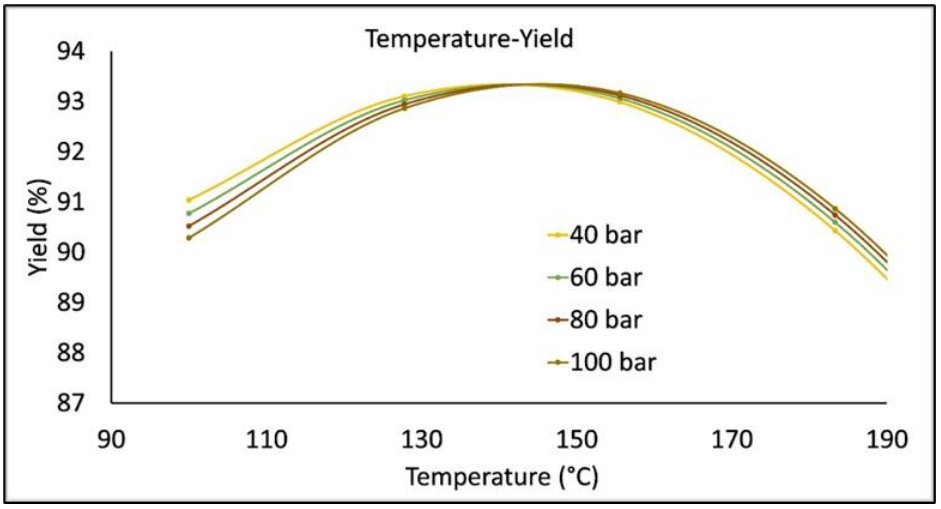

Figure 8. Yield of ammonia reactor under increasing temperatures with increasing pressures.

Upon examining the material flows in the table, it is observed that the output flow of the turbine named Turbine-3 contains hydrogen with a molar fraction of 99.8% in the vapor phase. Consequently, electrical energy is generated using the content values of the material flow named Turbine-3 Out, and this energy is recovered into the system to reduce the system's electrical energy requirement through a recovery method. Table 1 exhibits the mass temperature mass flow pressures and energy flow of the components in the whole system. T-1 Out, the output flow of the turbine named Turbine-1. This flow contains carbon monoxide with a molar fraction of 16.6% and carbon dioxide with a molar fraction of 83.3% in the vapor phase. To minimize environmental hazard, the pressure of this flow is reduced from 25 bar to 0.05 bar, and electrical energy is generated during the discharge process. This recovered energy is used to meet the electrical energy requirements of the element named PFRs (Ammonia Reactor).

Table 1. The parameters table of the simulation for each station.

Station	Mass Flow (kg/h)	Temperature (°C)	Pressure (bar)	Energy Flow (kW)
turbine-3 out	358,835	49.585	25	-161,064
flash sep-in	354,149	49.652	25	-159,658
vapor	358,835	85.586	87.5	-154,275
t-1 out	41,295.9	38.7701	0.05	-96,728.5
reactor 1 out	42,973.3	350	1.01	-95,707.2
comp sep 1 out	41,295.9	408.431	25	-91,741.9
water out	42,973.3	408.431	25	-89,127.4
comp 1 out	42,973.3	408.431	25	-89,127.4
CO+H2O	43,000	80.4529	1.01	-86,051.8
water	15,000	100	1.01	-55,357.6
co	28,000	25	1.01	-30,694.1
light liquid	4,107.08	172.09	87.5	-5,696.32
Tank outlet	4,107.08	172.09	87.5	-5,696.32
Turbine-2 out	8,792.73	250.518	150	313.146
Reactor out	87,92.73	425	200	20.4087
23	0	128.391	25	0
22	0	50	1.01	0
Pure N_2	7,115.4	200	25	357.892
cooler-1 out	1,677.33	200	25	1,180.95
mix-2 out	8,792.73	199.813	25	1,538.84
PURE H2	1,677.33	408.431	25	2,604.1
cooler 2 out	8,792.73	425	200	3,608.2
comp-2 out	8,792.73	573.718	200	4,968.34

Upon examining the energy consumption of the equipment within the system, in Table 2 it is notable that the element named Reactor 1 has a high energy consumption level (-9655.4 kW). However, this consumption is offset by the system's recovery methods, similar to how the energy needs of other equipment in the system are met. The energy requirements of system elements with high energy consumption, as discussed in the table, are addressed by using turbine elements within the system to expand material flows to the desired pressure. This expansion process also generates electrical energy, which is recovered to meet the system's energy needs.

Table 2. Energy balance of the system equipment.

Equipment	Type	Energy Consumption (-) / Generation (+) (kW)	MBR (kg/h)	EBR (kW)
Comp-2	Compressor	-6,788.81	0	-3,359.32
Comp-1	Compressor	-292.737	0	6,286.99

Flash Sep	Gas-Liquid Separator	-0.0291138	0.0207957	0.0291138
Ammonia storage	Tank	-4.28E-07	0	4.28E-07
Mix-2	Stream Mixer	4.86E-05	-3.20E-12	-4.86E-05
Mix-1	Stream Mixer	0.000699813	1.79E-10	-0.0006998
Compound Sep. 1	Compound Separator	10.3828	2.17E-10	4.00E-10
Turbine-2	Expander (Turbine)	292.737	0	-3.65E-07
Cooler-2	Cooler	1,360.14	0	1.28E-09
Cooler-1	Cooler	1,423.15	0	-8.54E-10
Ammonia reactor	Plug-Flow Reactor (PFR)	3,628.61	-5.72E-09	4.00E-08
Turbine-1	Expander (Turbine)	4,986.61	0	-8,615.22
Turbine-3	Expander (Turbine)	6,788.81	0	-0.0006232
Reactor 1	Gibbs Reactor	9,655.4	26,7317	-5.91E-08
Total Generation		11,775.42		
Total Consumption		-7,080.766		
NET BALANCE		4,694.654		

The reliability of the developed simulation model was verified by comparing the ammonia synthesis reactor performance with experimental data from the literature [10]. Figure 9 shows the comparison between simulated ammonia yields and experimental values across a temperature range of 250-400°C at constant pressure of 200 bar.

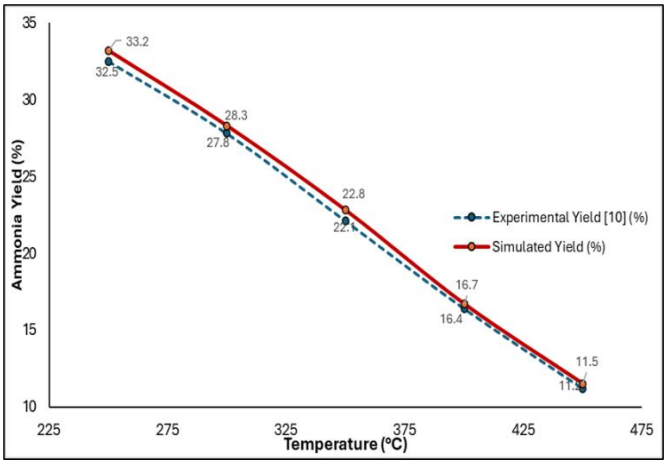

Figure 9. Model Validation: Ammonia Yield vs. Temperature

The close agreement between simulation results and experimental data, with an average relative error of 2.1%, demonstrates the accuracy of the Temkin-Pyzhev kinetic model implemented in DWSIM for ammonia synthesis. The maximum deviation observed was 3.4% at 350°C, which falls within acceptable limits for industrial process simulation.

4. CONCLUSION

In this study, the energy requirements of the Haber-Bosch process were met with an innovative energy recovery system, eliminating the need for an external energy source. Unlike traditional methods, the water-gas shift reaction was used to produce hydrogen from water molecules instead of natural gas. Carbon monoxide and carbon dioxide, which would otherwise be expelled as waste, were reintegrated into the process for recovery. The mass flow rates of unusable molecules were converted into electrical energy via turbines, enhancing the system's efficiency. Parametric studies were conducted to analyze the effects of temperature and pressure on yield and conversion rates in the ammonia reactor. These studies, illustrated with detailed graphs, highlighted the significant impact of temperature and mass flow on yield. The system was designed as a self-sustaining configuration that minimizes the environmental impact of harmful molecules by converting them into usable electrical energy. Compared to other systems, this design meets its energy needs through internal recovery and reduces the environmental carbon footprint by converting waste gases into electricity. In conclusion, this study introduces a sustainable and efficient framework for ammonia production, underscoring the critical role of integrated energy recovery and environmental stewardship in advancing green industrial processes.

REFERENCES

[1] M. Alsunousi and E. Kayabasi, "The role of hydrogen in synthetic fuel production strategies," Int. J. Hydrogen Energy, vol. 54, pp. 1169–1178, 2024. doi: 10.1016/j.ijhydene.2023.11.359.

[2] M. Klawitter, S. Wüthrich, P. Cartier, P. Albrecht, K. Herrmann, C. Gößnitzer et al., "Ammonia as a fuel: Optical investigation of turbulent flame propagation of NH_3/Air and $NH_3/H_2/N_2$/Air flames at engine conditions," Fuel, 2024. doi: 10.1016/j.fuel.2024.132616.

[3] N. Bora, A. Kumar Singh, P. Pal, U. Kumar Sahoo, D. Seth, D. Rathore et al., "Green ammonia production: Process technologies and challenges," Fuel, vol. 369, 2024. doi: 10.1016/j.fuel.2024.131808.

[4] A. G. Olabi, M. A. Abdelkareem, M. Al-Murisi, N. Shehata, A. H. Alami, A. Radwan et al., "Recent progress in Green Ammonia: Production, applications, assessment; barriers, and its role in achieving the sustainable development goals," Energy Convers. Manag., vol. 277, 2023. doi: 10.1016/j.enconman.2022.116594.

[5] M. J. Palys, H. Wang, Q. Zhang, and P. Daoutidis, "Renewable ammonia for sustainable energy and agriculture: vision and systems engineering opportunities," Curr. Opin. Chem. Eng., vol. 31, 2021. doi: 10.1016/j.coche.2020.100667.

[6] F. R. Bianchi and B. Bosio, "Modelling of green ammonia production based on solid oxide cells as electrolyser and oxygen separator for Haber-Bosch loop decarbonization," Int. J. Hydrogen Energy, 2024. doi: 10.1016/j.ijhydene.2024.07.047.

[7] P. Mayer, A. Ramirez, G. Pezzella, B. Winter, S. M. Sarathy, J. Gascon et al., "Blue and green ammonia production: A techno-economic and life cycle assessment perspective," iScience, vol. 26, 2023. doi: 10.1016/j.isci.2023.107389.

[8] M. Martín and A. Sánchez, "Biomass pathways to produce green ammonia and urea," Curr. Opin. Green Sustain. Chem., vol. 47, 2024. doi: 10.1016/j.cogsc.2024.100933.

[9] H. Nami, P. V. Hendriksen, and H. L. Frandsen, "Green ammonia production using current and emerging electrolysis technologies," Renew. Sustain. Energy Rev., vol. 199, p. 114517, 2024. doi: 10.1016/j.rser.2024.114517.

[10] D. A. Nowicki, G. D. Agnew, and J. T. S. Irvine, "Green ammonia production via the integration of a solid oxide electrolyser and a Haber-Bosch loop with a series of solid electrolyte oxygen pumps," Energy Convers. Manag., vol. 280, 2023. doi: 10.1016/j.enconman.2023.116816.

[11] A. F. Santos, "Natural Gas Production in the Brazilian Pre-Salt and Sustainable Development with the Generation of Blue Hydrogen and Blue Ammonia," presented at Day 3, Thu, October 26, 2023.

[12] I. Martínez, D. Armaroli, M. Gazzani, and M. C. Romano, "Integration of the Ca–Cu Process in Ammonia Production Plants," Ind. Eng. Chem. Res., vol. 56, pp. 2526–2539, 2017. doi: 10.1021/acs.iecr.6b04615.

[13] Z. Meng, X. Xu, W. Lin, B. Ge, Y. Xie, B. Song et al., "Role of ambient ammonia in particulate ammonium formation at a rural site in the North China Plain," Atmos. Chem. Phys., vol. 18, pp. 167–184, 2017.

[14] P. Li, Z. Jin, Z. Fang, and G. Yu, "A single-site iron catalyst with preoccupied active centers that achieves selective ammonia electrosynthesis from nitrate," Energy Environ. Sci., 2021.

[15] R. Lan, J. T. S. Irvine, and S. Tao, "Ammonia and related chemicals as potential indirect hydrogen storage materials," Int. J. Hydrogen Energy, vol. 37, pp. 1482–1494, 2012. doi: 10.1016/j.ijhydene.2011.10.004.

[16] V. Medina, H. Xiao, M. Owen-Jones, W. I. F. David, and P. J. Bowen, "Ammonia for power," Prog. Energy Combust. Sci., vol. 69, pp. 63–102, 2018. doi: 10.1016/j.pecs.2018.07.001.

[17] Y. Choi and H. G. Stenger, "Water gas shift reaction kinetics and reactor modeling for fuel cell grade hydrogen," J. Power Sources, vol. 124, pp. 432–439, 2003. doi: 10.1016/S0378-7753(03)00614-1.

[18] D. K. Lee, K. Y. Koo, D. J. Seo, and W. L. Yoon, "Analysis of design variables for an efficient natural gas steam reforming process comprised in a small scale hydrogen fueling station," Renew. Energy, vol. 42, pp. 234–242, 2012. doi: 10.1016/j.renene.2011.07.040.